ACS APPLIED MATERIALS & INTERFACES

Research Article

www.acsami.org

Green Synthesis of Asymmetrically Textured Silver Meso-Flowers (AgMFs) as Highly Sensitive SERS Substrates

Tran Thi Nhung and Sang-Wha Lee*

Department of Chemical and Biochemical Engineering, Gachon University San 64 Bokjeong-dong, Soojung-gu, Seongnam-si, Gyeonggi-do South Korea, 461-701

Supporting Information

ABSTRACT: Highly asymmetrical "flower-like" micron silver particles, so-called hierarchical silver meso-flowers (AgMFs), were facilely synthesized using ascorbic acid at room temperature in the presence of chitosan biopolymer. The time−evolution of TEM images and XRD analysis confirmed the anisotropic growth of AgMFs with single crystalline phase of which the formation mechanism was described in detail. The morphology and size of as-prepared AgMFs were tunable simply by changing the concentration of chitosan biopolymer and/or $AgNO_3$ precursor under otherwise identical conditions. The asymmetrically textured AgMFs dramatically enhanced Raman signals of probe molecules (2-chlorothiophenol, 4-aminothiophenol) even at a single particle level because of their surface morphologies consisting of numerous nanoedges and crevices.

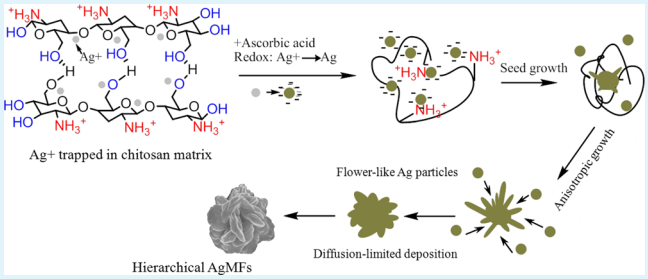

KEYWORDS: *chitosan, silver, meso-flowers, SERS, thiophenol*

1. INTRODUCTION

Surface-enhanced Raman scattering (SERS) technique has been intensively studied as a potent sensing platform in diagnostics.[1−4] It is generally recognized that the local electromagnetic (EM) effect contributes dominantly to the enormous enhancement of Raman scattering of probe molecules.[5−7] The EM effect arises from the collective oscillations of conductive electrons excited by the irradiated light on noble metal particles (Au, Ag, Pt, and Cu). Another partial contributor to the overall SERS signal is the chemical enhancement via the charge transfer (CT) mechanism. While the EM effect occurs at a certain distance from the surface, CT only occurs when the probe molecules directly adsorb on the metallic surface.[1−4,7] Because of the low chemical enhancement, most of sensor designs concentrate on the EM enhancement by exploiting complex topography of metallic nanostructures and/or controlling interparticle spacing as hot-spots.[8−11] The hot-spots are widely accepted to be responsible for dramatically enhanced local electromagnetic fields and in turn, amplifying Raman scattering of probe molecules in this region.

Recent researches have focused on developing numerous complex structures (such as dendrites, nanorods, prisms, triangles, wires, multipodes, stars, and flowers) as highly sensitive SERS substrates.[8,12−14] Among them, the hierarchical assembly of nanoscale building blocks into complex architectures is of great significance, for example, the assembly of one-dimensional nanorods/nanowires into branched nanostructures or starting from dispersed triangular nanoplates to ordered assemblies with anisotropic orientation.[15] These hierarchical nanostructures can display novel and collective physicochemical properties which are not found at the level of individual particles. However, the synthesis of hierarchical nanostructure still requires multiple steps, hazardous components, and even long fabrication times.

A variety of synthetic techniques have been reported to prepare hierarchical (or dendritic) metal nanostructures, such as electrochemical (or electroless) metal deposition, galvanic replacement, solvothermal (or hydrothermal) reaction, ultraviolet irradiation reduction, and ultrasonic-assisted reduction.[16−22] Unfortunately, most methods suffer from at least one of drawbacks such as long time-consuming, unclean particle surface, low reaction yield, and more importantly it is difficult to control the size and shape of the particles simply by adjusting the reaction parameters.[16,17] Recent studies have shown that wet-chemical synthesis, so-called colloidal chemical method,[18] is the low cost and high-yield route which can produce dendritic metal nanostructures using surfactant or polymeric template as either a growth controlling or a stabilizing agent.[16−19,21,23,24]

Nonetheless, the synthetic procedure of dendritic metal nanostructures usually takes long time in aging process[21,25] and is only feasible for some special kinds of synthetic polymers and surfactants.[18,26] For instance, polyvinylpyrrolidone (PVP) with pyrrolidone groups was proved as an effective capping agent in the synthesis of Ag dendrites when hydroxylamine was used as a reducing agent.[27] The formation of hierarchical nanostruc-

Received: September 14, 2014
Accepted: November 4, 2014
Published: November 4, 2014

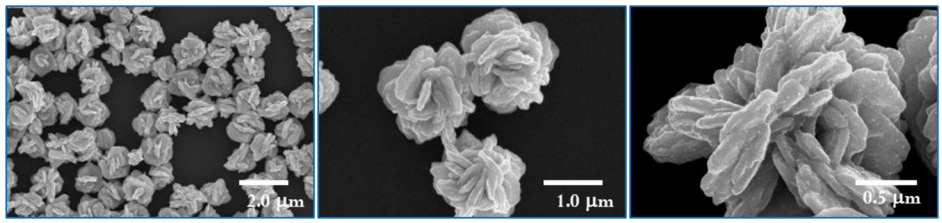

Figure 1. Typical SEM image of as-prepared AgMFs at different magnifications.

tures was also carried out using nonbiocompatible and toxic surfactants such as cetyltrimethylamonium chloride (CTAC), sodium dodecyl benzenesulfonate (SDBS), and tetrabutylamonium bromide (TBAB) which should be removed from the resulting particles for further biological applications.[28] Even though dramatic SERS effects have been reported on various dendritic Ag nanostructures, it is rare to find the green synthesis of highly asymmetrical Ag nanostructures using only biocompatible and nontoxic components.[19,24,26]

Herein, we report a facile nonhazardous synthetic route for highly nanotextured (i.e., asymmetric "flower-like") submicron Ag particles, so-called hierarchical silver meso-flowers (AgMFs). Chitosan biopolymer and ascorbic acid were used as a reducing and a structure directing agent, respectively, for the crystallographic growth of hierarchical AgMFs. Chitosan is known as a typical kind of natural polymer as a capping agent for the selective adsorption on favorable crystalline planes and induce the anisotropic growth toward that direction.[7,10,27,29] All the process takes the advantages of one-pot, fast, and green synthesis at room temperature. The surface morphology and size of as-prepared AgMFs were controllable simply by changing the concentration of chitosan or $AgNO_3$ precursor under otherwise identical conditions.

To explore the SERS enhancement of AgMFs, we used two small molecules with thiol groups, namely, 2-clorothiophenol (CTP) and 4-aminothiophenol (ATP). Thiophenol-type molecules have become increasingly important in SERS application as active Raman probes because of their strong binding to Au/Ag surface and their molecular electronics.[30,31] However, these molecules face with the problem of relatively small Raman cross-section which is challenging in the ultrasensitive detection by SERS technique, in contrast with other fluorescent dye molecules (e.g., rhodamine 6G, crystal violet, methylene blue). The hierarchical AgMFs showed a dramatic SERS enhancement even at an individual particle for both CTP (10^{-4}–10^{-6} M) and low ATP concentration (10^{-4}–10^{-8} M). Interestingly, at relatively high concentration of ATP (10^{-4}–10^{-6} M) the recorded Raman spectra were different from those obtained at low concentration of ATP (10^{-8} M), which were coincident with bulk ATP powder. This observation indicated the chemical conversion of ATP into 4,4′-dimercaptoazobenzene (DMAB) on the silver surface which has recently been reported as surface plasmon-driven catalysis.[31,32]

2. EXPERIMENTAL SECTION

2.1. Chemical. Chitosan (MW = 50 000) with the deacetylation degree of >85%, $AgNO_3$ (99.0%), L-ascorbic acid (99.0%), 2-clorothiophenol (CTP) (≥99%), and 4-aminothiophenol (4-ATP) (≥99%) were received from Sigma-Aldrich. Acetic acid (99.0%) was received from Duksan Pure Chem. Ltd., South Korea. All chemicals were used without further purification.

2.2. Synthesis and Sample Preparation. All glass wares were rinsed thoroughly by freshly prepared aqua regia solution (HCl/HNO_3 = 3:1) and rinsed again with distilled water prior to use. Chitosan of 1.0 wt % was dissolved in acetic acid solution (1.0 v/v%) by sonication until being transparent, followed by diluting with HPLC water. Subsequently, an aliquot (10–90 μL) of $AgNO_3$ (1.0 M) was added into 3 mL of chitosan solution under vigorous stirring for 5 min. Finally, asymmetrical flower-like Ag microns (or hierarchal Ag meso-flowers) were obtained by adding ascorbic acid (1.0 M) of 60 μL to the mixed solution and kept stirring for 10 min. The resultant Ag meso-flowers (AgMFs) were purified by three consecutive centrifugation-sonication steps and resuspended in HPLC water.

For SERS analysis, an aliquot of CTP molecules with different concentrations were added to an equal volume of as-prepared AgMFs. The mixture was shaken for a few minutes and allowed to stand still at room temperature for 4 h to obtain the equilibrium adsorption of CTP on AgMFs. The subsequent centrifugation removed excessive and loosely bound CTP and resuspended in diluted HPLC water. Finally, a drop of CTP-bound AgMFs solution was casted on a well-cleaned silicon slide and let them dry statically at room temperature prior to SERS measurements. The same procedure was applied to 4-aminothiophenol (ATP) in SERS measurements, except for that ATP-bound AgMFs were suspended in ethanol.

2.3. Analytical Instruments. The size and morphology of as-prepared AgMFs were characterized by Scanning Electron Microscope (SEM, S-4700 Hitachi) at the excitation electron beam of 15 keV and Transmission Electron Microscope (TEM) at the accelerating voltage of 300 kV (HITACHI, H7600). X-ray diffraction (XRD; Rigaku Corp.) with Cu Kα radiation was used to examine the crystallographic structure of solid samples. UV–vis spectrometer (CARY) and the Raman spectroscopy (LabRam HR) were employed to characterize the optical properties of as-prepared samples. The Raman spectrograph employed 1800 g/mm grating and He–Ne laser excitation at 632.8 nm.

3. RESULTS AND DISCUSSION

3.1. Synthesis and Characterization of Hierarchical AgMFs. Highly asymmetric "flower-like" AgMFs (i.e., hierarchical AgMFs) were obtained a few minutes after starting the reduction of $AgNO_3$ in the presence of ascorbic acid and chitosan at room temperature. The ascorbic acid is a mild reducing agent, known as a vitamin C, which is widely used in the synthesis of various complex nanostructures.[15,24,33] Chitosan is a biocompatible polymer containing primary amine and hydroxyl groups which have high affinity to Ag nanoparticles. Chitosan unraveled the ability in fabricating complex nanostructures as a capping and shape-controlling agent.[7,10,27,29]

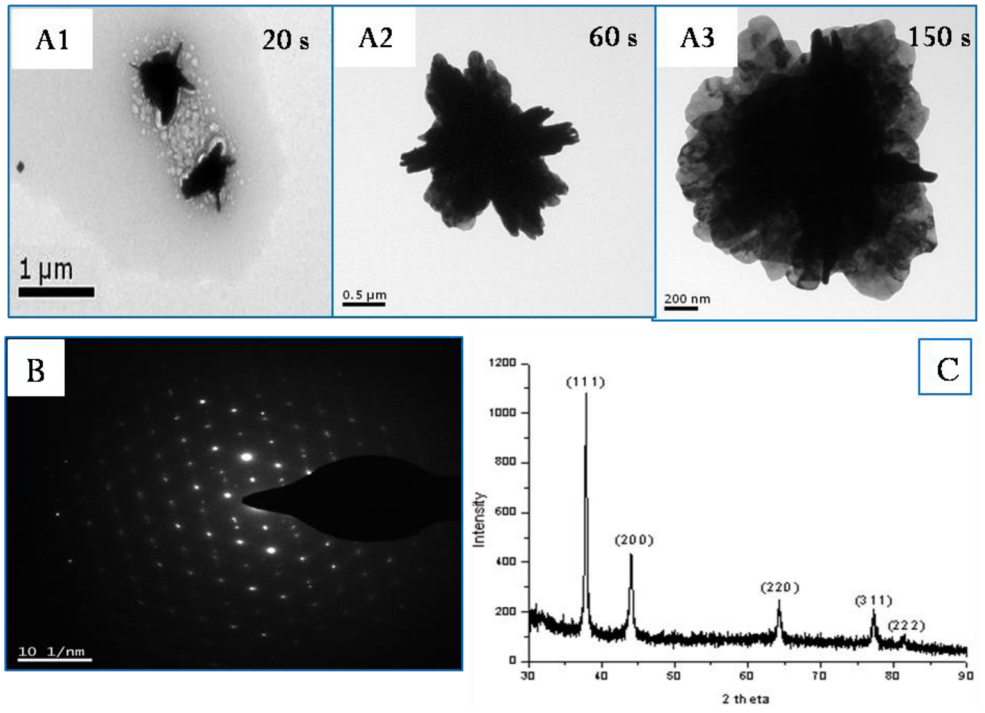

Figure 2. TEM images of as-prepared AgMFs sampled at predetermined times at (A1) 20 s, (A2) 60 s, (A3) 150 s, (B) SEAD pattern of the AgMFs, (C) XRD spectrum of the AgMFs.

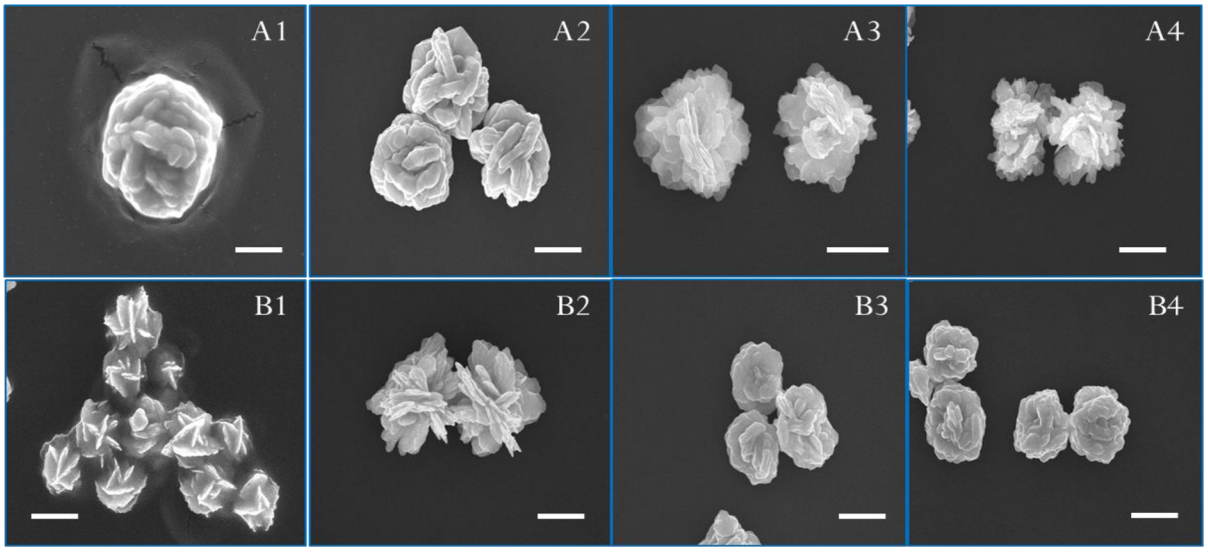

Figure 3. SEM images of AgMFs prepared by different concentrations of chitosan at fixed volume of added $AgNO_3$ (60 μL from a 1.0 M stock solution) (A1, 0.05 wt %; A2, 0.1 wt %; A3, 0.3 wt %, A4, 0.4 wt %), and different amounts of $AgNO_3$ (upon the addition of different volumes from a 1.0 M stock solution) in the presence of 0.1 wt % chitosan (B1, 10 μL; B2, 30 μL; B3, 60 μL; B4, 90 μL). All scale bars are 1 μm.

Figure 1 shows the typical SEM images of hierarchal AgMFs at different resolutions. As shown in Figure 1, the AgMFs exhibited a good size distribution (~1400 nm). The magnified SEM images apparently revealed that the AgMFs had highly nanotextured surface morphologies. The hierarchal AgMFs exhibited spherical grain boundary and stacking rod-shaped edges with ~50−100 nm in width, but not uniform in length. In particular, as-prepared AgMFs exhibited three-dimensional (3-D) hierarchical assemblies of roughened nanoscale edges which are quite different from relatively symmetrical Ag dendrites prepared by many groups.[7,11,15,23−25,34−36]

To get an insight for the growth mechanism of as-prepared samples, the morphology of AgMFs was recorded by TEM images taken at different growth times (20, 60, and 150 s). The AgMFs were prepared by stopping the reaction at predetermined times (i.e., diluting the solution by 20 times) and removing the unreacted components by the immediate centrifugation at 10000 rpm for 1 min. The significant changes of the morphology at different growth times were apparently observed by time-evolution TEM images, that is, the transition from the irregular particles (Figure 2A1) to dendritic multiple-branched particles (Figure 2A2), and even to hierarchical submicron flower-like particles (Figure 2A3). The dark contrast

Scheme 1. Proposed Mechanism Illustrates the Formation of Hierarchical AgMFs

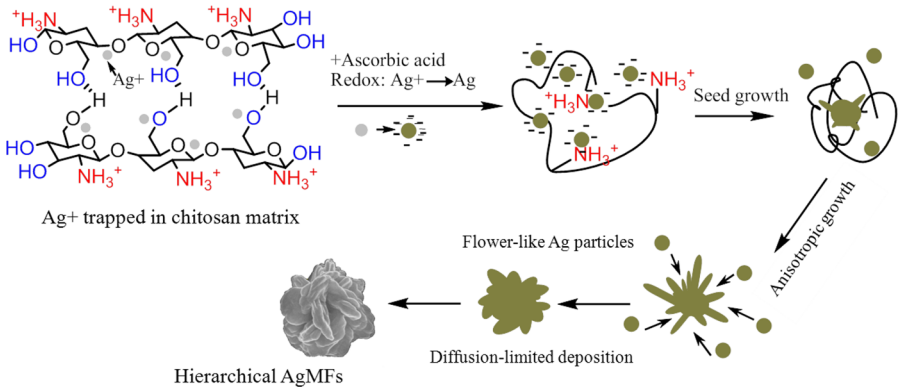

at the body center indicated that the resultant AuMFs were rich in 3D structure. The particles exhibited a homocentric growth in which some elementary branch was initially formed and served as a skeleton for the secondary deposition of Ag^0 atoms and thereby forming multiple thin sheets over the surface. Selected area electron diffraction (SAED) analysis confirmed the single crystalline structure of AgMFs (see Figure 3B), in contrast with polycrystalline structures of nanotextured silver microflowers synthesized in the absence of chitosan.[36] The X-ray diffraction (XRD) spectrum of the sample showed five sharp peaks corresponding to {111}, {200}, {220}, {311}, and {222} facets (see Figure 2 C) attributed to face centered crystal (fcc) Ag particles.[17] Noteworthy, the intensity of (111) diffraction peak was much higher than those of other peaks, indicating that hierarchical AgMFs had plenty of {111} facets and the crystal growth preferentially oriented parallel to the {111} facets.[16,17,25]

XPS survey and EDX data confirmed the existence of O, C, N elements on AgMFs which originated from adsorbed chitosan and/or oxidized components from ambient environments (Figure S1 in the Supporting Information). Due to the interaction of Ag and functional groups ($-NH_2$, $-OH$) of chitosan molecules, some chitosan are still intact on the surface of AgMFs to prevent the particle from agglomeration. However, it is unlikely for the chitosan to be embedded inside the crystal structure of Ag particles because the Ag particle showed the perfect single crystallographic structure confirmed by XRD and SAED analysis as shown in Figure 2. If the chitosan is embedded inside the Ag particle, it may generate dislocations and defects in the crystalline structure of Ag particles.

The common mechanisms to control the morphologies of synthesized particles are kinetic controlling and surface passivation pathways.[37] It has been reported that kinetically controlled reaction can be established by slowing down the reduction rate which is responsible for generating nanostructures containing low-index facets such as {111}, {100}, {110}.[18,37] In general, the complexation of Ag^+ ions with chitosan chains via coordinate bonding with amine and hydroxyl groups varies the reduction potential of Ag^+ and consequently changes the redox rate of $AgNO_3$ to Ag^0. In terms of surface passivation pathway, like other conventional structure-directing agents, chitosan can selectively bind to certain crystal facets, altering the order of free energies at different facets and thereby influencing on their crystal growth.[38] As a result, released Ag^0 was added to unpassivated facets until the final particle was dominantly covered by passivated facets.[37,38] However, in our protocol, the growth mechanism became more complicated due to the large number of different functional groups of chitosan, in contrast with other structure directing agents (PVP, CTAB, citrate) which have a limited number of functional groups. Free functional groups in chitosan when it selectively bound to certain crystal facets can attract Ag^0 atoms from the solution, resulting in stacking growth of nanosheets to form highly asymmetric Ag nanostructures. This phenomenon is very similar to the scrolling action of chitosan chains in the formation of gold nanoflowers.[39] Therefore, chitosan or other polysaccharide polymers could be ideal surfactants to form complex nanostructures with anisotropic morphology.[7,40,41]

To examine the effect of chitosan concentrations on the formation of resultant AgMFs, a series of experiments was conducted by varying the chitosan concentration under otherwise identical condition. The morphology and size of AgMFs were strongly influenced by chitosan concentration, as shown in Figure 3A1−4. The fast color changes from transparent to gray, dark gray and turbid were observed within a few minutes immediately after adding ascorbic acid into the vigorously stirring mixture of $AgNO_3$ and chitosan. At the high concentration of chitosan (0.3−0.4 wt %), SEM images shown in Figure 3A3−4 represented a distinct hierarchical architecture with well-separated multiple petal assembly. The petals exhibited a homocentric form composed of numerous protuberances originated from the deposition of Ag^0 atoms. The morphology and size of AgMFs were obviously changed when the chitosan concentration was reduced to 0.1−0.05 wt % (see Figure 3A1−2). The AgMFs appeared to have spherical grain boundaries consisting of many roughened nanoedges and nanodots generated by the traces of disappeared nanosheets. Consequently, the crystallographic growth of dendritic AgMFs was well-controlled, that is, chitosan not only played as a capping agent but also controlled the shape and size of resulting particles.

The anisotropic growth of Ag particles was also controlled by Ag^+ ions because the concentration of $AgNO_3$ influenced on the rates of nucleation and growth process.[17,26,42] The dosage amounts of $AgNO_3$ (1.0 M) were varied to examine the concentration effect of Ag^+ ions on the characteristic morphologies of AgMFs. Figure 3B1−4 is the SEM images showing the morphology changes of AgMFs with the increase of $AgNO_3$. At low dosage amounts (10−30 μL) of $AgNO_3$ (shown in Figure 3B1−2), the morphology of AgMFs appeared quite similar to those obtained at high concentration of chitosan (A3 and A4), consisting of numerous thin single petals

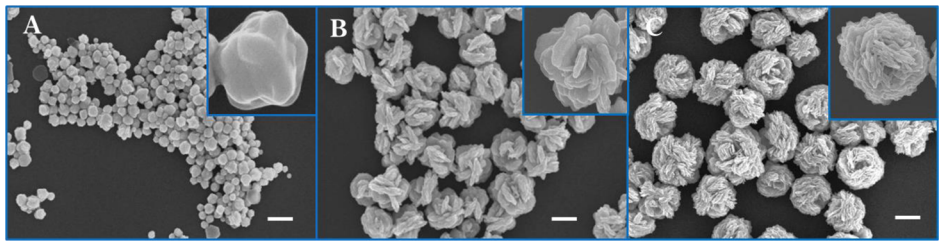

Figure 4. SEM images of AgMFs prepared at different reaction temperatures under fixed amounts of added ascorbic acid (60 μL from a 1.0 M stock solution) and chitosan of 0.1 wt %: (A) High temperature (60 °C), (B) medium temperature (25 °C), and (C) low temperature (4 °C). All scale bars are 1 μm.

with different lengths. An apparent morphology change to roughened surface consisting of edges and nanodots occurred when increasing the dosage amounts of $AgNO_3$ up to 60−90 μL (see Figure 3B3−4). It is probably because of the gradual deposition of Ag^0 atoms on thin petals and crevices to form thicker petals until they became roughened edges.[18,43]

In summary, chitosan concentration and dosage amounts of $AgNO_3$ are key factors which can control the anisotropic growth of resultant Ag particles (vide infra). The increase of chitosan concentration decreased the size of AgMFs with more roughened hierarchical architecture, whereas the increase of $AgNO_3$ induced more roughened surface morphology without distinct size changes of the particles. The binding affinity of chitosan, which contains abundant functional groups of amine and hydroxyl groups, varies at different crystal facets, consequently leading to the formation of Ag nanostructures with complex topography.

On the other hand, silver nitrate concentrations usually determine Ag ion availability in the reaction mixture and controlled the growth rates of Ag particles. Interestingly, the concave structures among sheets might be more energetically favorable in the formation of Ag particles by adding silver precursors.[38] At higher concentration of silver nitrates, the silver atoms tended to fill the spaces among sheets to form roughened surface morphology. Conclusively, silver nitrates and chitosan complementarily control the anisotropic growth, resulting in hierarchical AgMFs.[37]

Scheme 1 represented the proposed mechanism in the formation of hierarchical AgMFs by the ascorbic acid and chitosan biopolymers. At first, primary Ag^0 atoms were slowly released from the reduction of Ag^+ ions trapped in the chitosan matrix through the complexation with functional groups. These Ag atoms were quickly aggregated during the nucleation process to form initial seeds to reduce the interfacial free energy, assisted by the scrolling action of chitosan chains. These newly formed seeds were stabilized in the chitosan matrix by the extra-repulsive forces between positively charged chitosan chains adsorbed on different Ag seeds. The selective adsorption of chitosan varies the surface energy of different facets. However, the presence of chitosan at Ag/solvent interface did not seem to interfere with diffusion-limited deposition of Ag^0 atoms onto seed particles, probably due to favorable attractive forces between positive amine groups of chitosan and negative surface of Ag^0 atoms. Subsequently, these seeds acted as the center to capture free Ag^0 atoms from the solution, leading to the crystallographic growth into hierarchical AgMFs. With the increase of reaction times, other free Ag^0 atoms diffused continually toward the hierarchical and further deposit on empty surface of branches, finally forming thicker branches and roughened surfaces on Ag particles.

Because the kinetically controlled reaction occurs far from equilibrium state, a small change of reaction temperature can amplify the difference in the growth rates of individual crystal facets, consequently affecting the morphology and size of resultant crystalline structure.[18,43] To confirm this supposition, three different reaction temperatures were selected: high temperature (60 °C), medium temperature (25 °C), and low temperature (4 °C). The reaction temperature ranges were far below the glass transition temperature of chitosan polymers (140−150 °C).[44] Therefore, the thermal effect of reaction temperature on the structural properties of chitosan polymers might be negligible. According to the SEM images shown in Figure 4, the size and morphological complexity of resultant particles changed significantly when lowering the reaction temperature. At high temperature, the as-synthesized Ag particles appeared quasi-spherical structure with relatively small size (Figure 4A). High temperature promoted the reaction rates and diffusion of components, consequently leading to the rapid formation of corpuscular nanostructures.[15]

Notably, lower temperature produced more complex Ag nanostructures by slowing down the reaction kinetics and diffusion rates.[10,45] When compared to the surface morphology of AgMFs at 25 °C, AgMFs at 4 °C exhibited more complex morphology with thinner and shorter edges. The slower diffusion rate at lower temperature induced more supersaturation of reactive species so that the nucleation and crystallographic growth times were prolonged, resulting in highly complex morphology of Ag particles.[15,46]

As previously mentioned, many approaches utilized non-biocompatible surfactants and co-operative agents for the selective surface passivation to induce the dendritic or branched Ag particles.[6,11,16−19,21−26] For instance, hierarchical Ag nanostructures were formed using PVP surfactant and SDS (or PDP) which were not biocompatible, requiring the additional purification process to minimize the possible contaminations in the biological applications.[6,47,48] In addition, most Ag nanostructures were usually classified as symmetrical dendrites or metallic nanostructures formed by the aggregation of primary nanoparticles with polycrystalline phases.[49,50] In this work, we synthesized flower-like Ag particles using the one-pot, fast, and green synthesis at room temperature and the resulting particles exhibited highly asymmetric nanostructures with single crystalline phases.

3.2. Optical Properties of AgMFs. It is well-known that the optical properties of metal nanoparticles are highly affected by their size, shape, and composition. Size and shape of NPs are crucial factors determining the number, the shape, and the positions of localized surface plasmon resonance (LSPR) peaks in the extinction spectra.[21,24,51] For example, nonspherical Ag NPs (such as triangle, branched, rod) usually display several

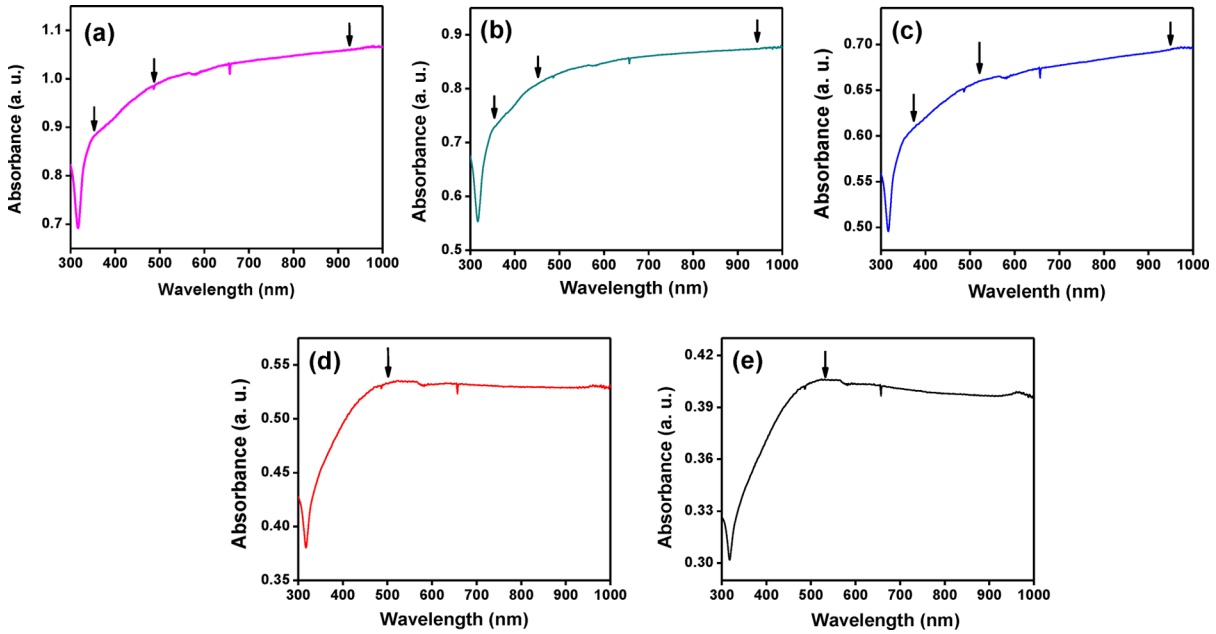

Figure 5. UV−vis spectra of AgMFs (25 °C) prepared at 60 μL of ascorbic acids (1.0 M) with different chitosan concentrations: (a) 0.4, (b) 0.3, (c) 0.2, (d) 0.1, and (e) 0.05 wt %.

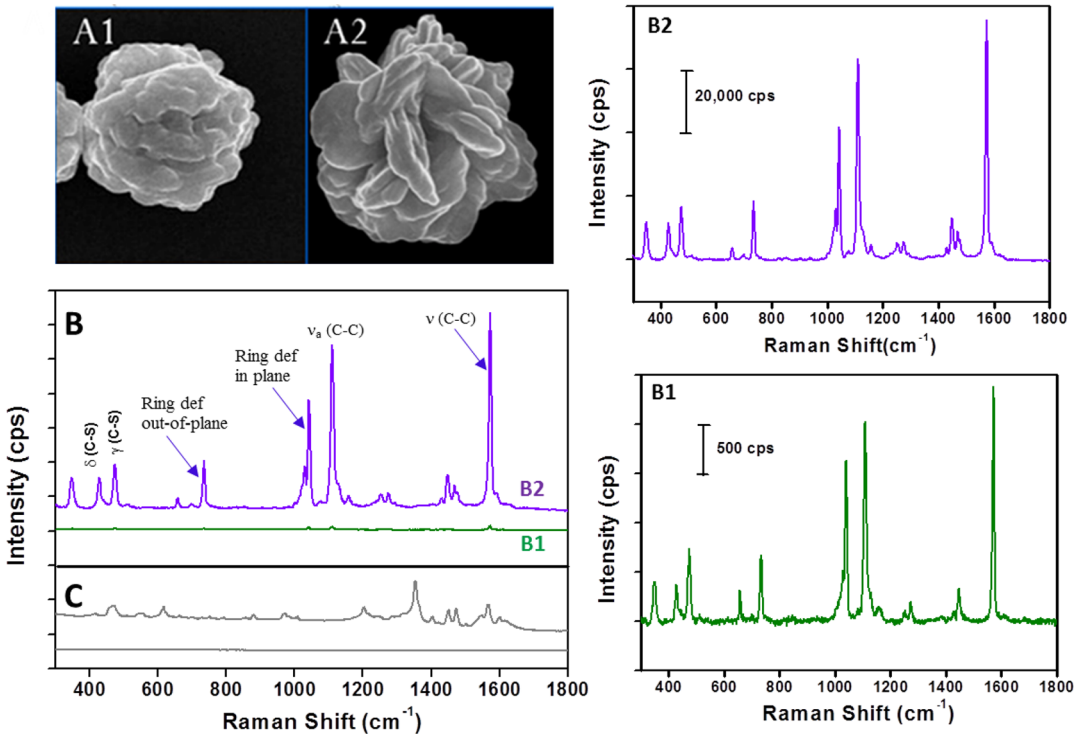

Figure 6. Efffect of surface morphology of AgMFs on the SERS efficiency: (A1, A2) SEM images of AgM6 type 1 and type 2; (B) SERS spectra of 2-chlorothiolphenol (CTP) on two distinguished AgMFs corresponding to (A1) and (A2); (C) SERS spectra of bare AgMFs at two different places; (B1, B2) the enlarged Raman spectra shown in (B). All spectra was recorded by 632.8 nm excitation laser (10 μW) with the integration time (60 s) and one accumulation for 500 counts per division in (B1) and 20000 counts per division in (B2).

LSPR peaks because of the in-plane and out-of-plane dipolar oscillations of free electrons whereas spherical Ag NPs exhibit only one peak at around 420 nm.[7,49,51] As the particle become less symmetric, the induced charge distribution can result in not only dipolar modes with different frequencies but also the multiple modes of LSPR peaks.[52]

Figure 5 shows the UV−vis spectra of AgMFs synthesized at different chitosan concentrations. All the spectra exhibited the similar broad absorption bands ranged from 420 nm to NIR region regardless of the morphology and size of AgMFs. The higher-ordered multipole plasmon resonance peaks were observed in addition to the dipole resonance peak at high chitosan concentration, probably due to the multiple thin

sheets in Ag nanostructure. These peaks gradually disappeared when the concentration of chitosan decreased from 0.4 to 0.2 wt %. At the lower concentrations of chitosan (0.1−0.05 wt %), the UV−vis spectra displayed only one clear absorption peak around 520 nm which was fairly red-shifted in reference to the absorption peak of spherical Ag NPs around 410 nm, probably due to the bigger size and roughened surface.[53] As the same analogy, a very similar trend in the UV−vis spectra was observed when increasing the dosage amounts of $AgNO_3$ (1.0 M) (Figure S2 in the Supporting Information).

3.3. SERS Detection of 2-Chlorothiophenol. Raman spectroscopy is a highly specific technique, which can detect and identify probe molecules based on their vibrational energy levels as Raman fingerprints. Because the Raman enhancement factor was low ($\sim 10^3$) for a metallic particle with a smooth surface,[5,54] many efforts have focused on the synthesis of complex nanostructures with many hot-spots which can markedly enhance Raman signals up to 10^8−10^{12}. The hierarchical organization of AgMFs are believed to highly impact on the Raman enhancement of probe molecules.[8]

An enhancement factor (EF) is the index which can represent the relative sensitivity of the substrate in SERS measurement. According to the EF calculation for a single particle, it is crucial to accurately estimate the number of adsorbed molecules on the particle surface based on the self-assembled monolayers (SAMs) which do not usually depend on the bulk concentration of probe molecules. In this work, the initial bulk concentration of CTP was kept high (10^{-4} M) enough to guarantee the saturated adsorption of CTP on the Ag surface.

To explore the effect of morphology on SERS sensitivity to 2-chlorothiophenol (CTP), two types of AgMFs (shown in Figure 6A1 and 6A2) were chosen. The first one had spherical-like grain boundary structure with roughened surface, whereas the latter one had an asymmetric hierarchal structure with a large number of randomly oriented thorny protrusions and tiny cavities. SERS sensitivity of these particles was assessed by 2-chlorothiophenol (CTP) molecules which can chemisorb on the surface of AgMFs via thiol groups. To investigate the SERS sensitivity of flower-like Ag particles, AgMFs were incubated in CTP solution for a sufficient time to obtain a saturated adsorption of CTP on the surface of AgMFs through strong Ag−S bindings. The subsequent centrifugation of CTP-bound AgMFs was thoroughly conducted in order to remove excessive and loosely bound CTP from the particle surface. Only the self-assembled monolayer of CTP on the AgMFs was retained on the Ag surface after the purification step. Finally, an aliquot of CTP-bound AgMFs was dropped and casted over a well-cleaned silicon slide, fully air-dried before SERS measurements.

The Raman intrument was operated at integration time of 60 s, one accumulation, and 632.8 nm excitation laser (10 μW). Normally, higher numbers of accumulation cycles and long integration times result in strong intensity and better resolution of Raman signals due to higher signal/noise ratio. However, long exposure time along with a strong laser power might cause sample degradation, especially for fragile biosamples. Therefore, instrumental parameters must be carefully chosen to balance between signal maximization and minimization of sample degradation. In this work, the exposure time of 60 s (one cycle of accumulation and 60 s of integration time) was appropriate to get SERS signals of CTP at the low power density of 1×10^3 W/cm^2 (10 μW per 1.0 μm^2).

Figure 6B1 and 6B2 showed the SERS spectra of CTP adsorbed on two types of AgMFs (6A1 and A2). In both cases, the typical SERS peaks of CTP were distinctly enhanced at 1025, 1120, and 1580 cm^{-1}, demonstrating the efficient encoding process of CTP on both types of AgMFs. However, the asymmetrcial AgMFs (6A2) exhibited a significant enhancement in SERS spectra of CTP when compared to the less asymmetrcial AgMFs (6A1). The relative enhancement was ca. 50 times based on the peak intensity at 1042, 1110, and 1573 cm^{-1}.[39] The reason may be that a large number of tiny cavities and randomlly oriented nanoprotrusions induced the dramatical enhancement of electromagnetic fields. This feature was previously observed in sharp edge or branched metal nanostructure.[30,35,55] The rough AgMFs also displayed much higher SERS enhancement to 4-aminothiophenol (ATP) than the smooth AgMFs prepared at hot temperature (Figure S4 in the Supporting Information).

Figure 6C showed the SERS spectra of bare AgMFs without CTP at differnet positions. Since AgMFs were rinsed with HPLC water, no noticeable signal in SERS spectrum was observed at one position (Figure 6C). At the other position, however, there was an appearance of Raman signals which might be originated from the susceptibility of Ag particles to ambient environments.[56] However, it would not impair the SERS efficiency of CTP detection because the position and intensity of all Raman peaks are different from those of CTP peaks. It is worth mentioning that the appearance of chitosans on the surface of AgMFs did not give noticeable noisy peaks in the SERS detection of CTP, as well as it did not block the adsorption of CTP on the surface of AgMFs.[7,10]

Because of the complex surface morphology of AgMFs and a limited sensitivity of SERS system, an EF enhancement factor was roughly calculated based on the following eq 1:[57]

$$\mathrm{EF} = \frac{I_{\mathrm{SERS}} \times N_{\mathrm{bulk}}}{N_{\mathrm{SERS}} \times I_{\mathrm{bulk}}} \quad (1)$$

Here, I_{SERS} and I_{bulk} are the intensity of a vibration mode in the SERS spectrum of adsorbed probes and in the Raman spectrum of bulk solution of probes, respectively. N_{SERS} is the number of molecules adsorbed on the silver particles within the laser spot size and can be calculated by eq 2[50]

$$N_{\mathrm{SERS}} = N_{\mathrm{AV}} \in S_{\mathrm{f}}\sigma,\ S_{\mathrm{f}} = \pi\left(\frac{{d_{\mathrm{f}}}^2}{4}\right) \quad (2)$$

where N_{AV} is the Avogadro number and S_{f} is the effective surface area of metallic structure within the spot size, and σ is the surface density of self-assembled monolayers of CTP molecules. Based on the assumption that only a self-assembled monolayer of CTP is retained on the surface after the purification step, the total number of chemisorbed molecules can be calculated theoretically regardless of the initial bulk concentration of CTP (10^{-4} M) in this work. The nominal surface area was calculated based on the spot size ($d_{\mathrm{f}} = 0.86$ μm, 100× objective lens) which was less than the footprint size of single AgMFs, and the shape factor, ε, was assumed to be ∼10 because of the combined effect of increased surface area and the shaded fraction of surface area due to the complex surface morphology.[5]

The surface density of *p*-fluorothiolphenol (*p*-FTP) on a noble metal surface was reported as ∼0.44 nmol/cm^2 assuming a self-assembled monolayer (SAM), which is very similar to the surface density of thiophenol (TP) on the metal surface.[58,59]

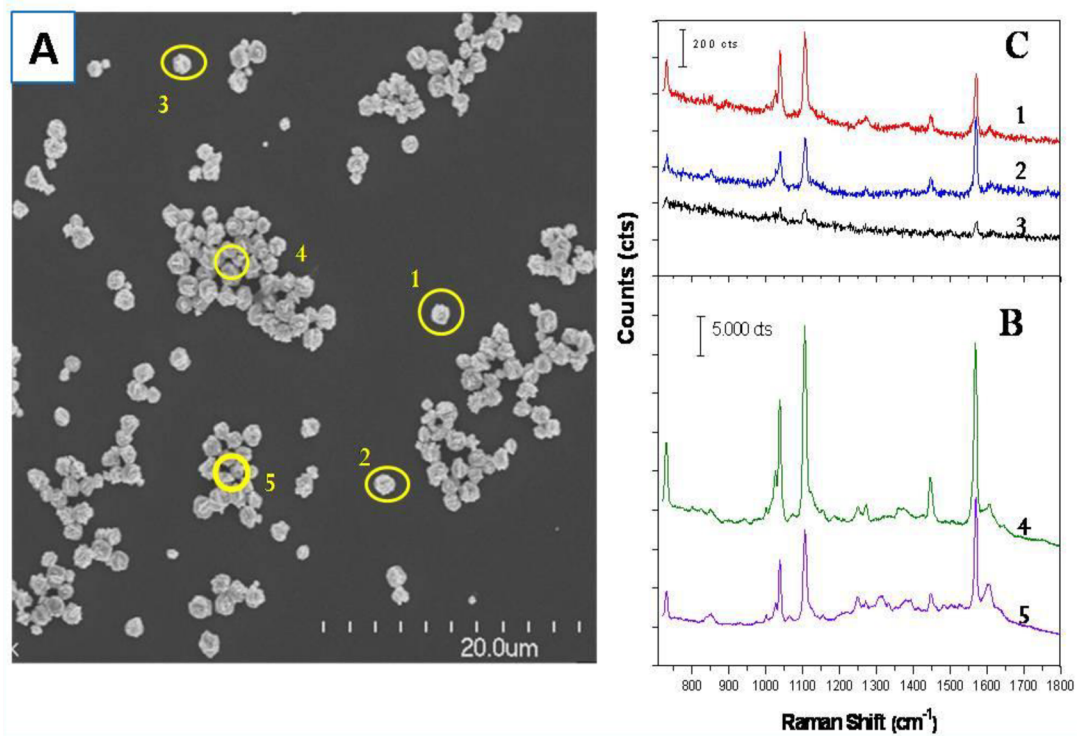

Figure 7. (A) SEM image of as-prepared AgMFs spreaded on the silicon slice. (B) SERS spectrum of 2-chlorothiophenol adsorbed on the AgMFs at two differently aggregated places marked as 4, 5 in panel A. (C) SERS spectra of 2-clorothiophenol (CTP) adsorbed on three different isolated particles marked as 1, 2, 3 in (A). All spectra was recorded by 632.8 nm excitation laser (10 μW) with the integration time (60 s) and one accumulation for 200 counts per division in (C) and 5000 counts per division in (B).

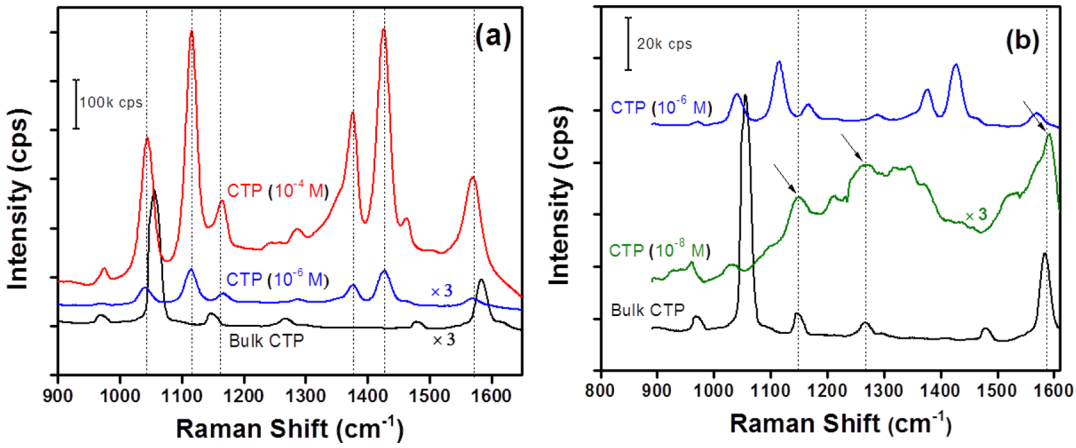

Figure 8. Comparison of Raman spectra of ATP adsorbed on AgMFs taken at different concentration ranges: (a) 10^{-4}–10^{-6} M and (b) 10^{-6}–10^{-8} M. Only these spectra were recorded by micro-Raman (ANDOR Monora500i) equipped with 633 nm He–Ne laser (12 mW) for 50 s of integration time and one cycle of accumulation.

According to the recent work by Jiang et al., the *o*-fluorothiolphenol (*o*-FTP) SAMs has a lower surface coverage by ~40% than that of *p*-FTP SAMs because of the different molecular geometry and intermolecular electrostatic interactions.[59] As the same analogy, the surface density of 2-chlorothiophenol (CTP) on the metal surface would be assumed as ~0.2 nmol/cm^2 which was 40–50% of the reported value of thiophenol. The chlorine atoms at the ortho position of benzene rings usually induce more tilting from the substrate surface, consequently leading to loosened SAMs density.[60] On the basis of the comparable surface density (σ) of CTP, the total number of adsorbed molecules on the metal surface was calculated as 6.99×10^6.

The total number of CTP molecules, N_{bulk}, in the focal volume of bulk solution can be calculated by eq 3[40]

$$N_{bulk} = N_{Av} V_f \frac{\rho}{M_{wt}}, \; V_f = \pi \left(\frac{{d_f}^2}{4} \right) h_f \tag{3}$$

where ρ is the density of CTP molecules (1.275 g/cm^3) and M_{wt} is the molar mass of CTP molecules (144.62 g/mol). The focal volume, V_f, illuminated by the focused laser, in which d_f is the diameter of focused spot (3.1 μm, 10× objective) and $h_f \cong 4\lambda/(\mathrm{NA})^2$ is the depth of focus.[61] In our protocol, h_f is about 40.5 μm with 10× objective lens (numerical aperture, NA = 0.25) and λ = 632.8 nm excitation wavelength. Then, the total

number of bulk molecules within the probing volume of solution phase would be 16.2×10^{11}. On the basis of the SERS and Raman peaks of CTP at 1121 and 1578 cm^{-1} shown in Figure 6B and Figure S1 (in the Supporting Information), the average EF was calculated as 3.7×10^7. This value is ranged within the highest EF values that have been reported for thiophenol-type molecules on similar flower-like Au/Ag nanostructures.[5,30,35,62]

As shown in the SEM image of Figure 7A, isolated particles and aggregated AgMFs coexisited. In practice, the adsorption and film forming of chitosan on the silicon slide after solvent evaporation can hamper the heavy agglomeration of AgMFs.[7] Figure 7C showed the distinct SERS spectra of CTP molecules adsorbed on three isolated AgMFs at the position of 1, 2, and 3 in the SEM micrograph. It should be noted that SERS signals represent the average values over the whole surface of each particle, and that highly localized protrusions or inside the crevices of each particle's surface can provide dramatic increase of SERS signals.[5,6] As shown in Figure 7B, a significant increase of SERS signals were observed on the aggregated AgMFs at the position of 4 and 5. Conclusively, the aggregated AgMFs exhibited the more enhancement of SERS signals by ~100 times higher than those of individual AgMFs. It is because of a large number of plasmon gaps between adjacent particles, so-called hot-spots, give additional enhancement to the inherent electromagnetic (EM) fields of individual particles.[5,6] The aggregated AgMFs demonstrated the EF value even up to $10^8 \sim 10^9$ over the highest values that have been reported for thiophenol-type molecules.[5,50,61,63,64]

3.4. SERS Studies of 4-Aminothiophenol (ATP). We conducted the Raman measurement of 4-aminothiophenol (ATP) adsorbed on hierarchical AgMFs according to the aforementioned protocol conducted for CTP detection. Figure 8 shows the SERS signals of ATP adsorbed on hierarchical AgMFs at different concentration ranges from 10^{-4} to 10^{-8} M, as well as bulk ATP powder. As seen from Figure 8a, SERS measurements of ATP (10^{-4} M and 10^{-6} M) displayed the distinct peaks at 1110, 1375, and 1425 cm^{-1}, which were not observed from bulk ATP powder. The disagrement of SERS signals indicated the feasible conversion of neighboring ATPs on the silver surface into 4−4′-dimercaptoazobenzen (DMAB) under high power laser (633 nm of He−Ne laser, 12 mW).[65]

The chemical dimerization of 4-aminothiophenol (ATP) adsorbed on a roughened silver surface into DMAB was recently observed in SERS signals under continuous laser exposure or increasing the power density of a laser.[31,32,65] The chemical reaction was attributed to the hot electrons generated from the surface plasmon excitation or the local plasmon heating on silver nanoparticles in coexistence with O_2/H_2O.[32] Although the reaction mechanism is not fully understood yet, the crucial role of silver nanoparticle as a surface plasmon-assisted catalyst is undoubted.

On the other hand, SERS measurements of ATP (10^{-8} M) rather displayed some coincident Raman bands with those of bulk ATP powder, as seen from Figure 8b. It is plausible to assume that low density of ATP molecules on the silver surface is a major reason for ATP not to be dimerized into DMAB. Thus, our AgMFs detected ATP molecules at the very low concentration level in spite of comparable noise signals in SERS measurements. To be conslusive, our AgMFs showed highly sensitive detection of ATP (10^{-8} M) and feasible plasmon catalyst for ATP (10^{-4}−10^{-6} M) owing to their unique morphology which can induce tremendous SERS enhancement.

4. CONCLUSIONS

In this work, we demonstrated a facile and green synthetic route for preparing submicron dendritic (hierarchical flower-like) Ag particles (AgMFs). In this synthetic procedure, chitosan biopolymer played an important role as a stabilizer and a structure-directing agent, supporting for the anisotropic growth of AgMFs. The morphology organization of AgMFs with a large number of protrusions and crevices was simply tunable by changing the concentration of chitosan or dosage amounts of $AgNO_3$ at room temperature. The AgMFs as an individual particle was highly sensitive in SERS measurement in the detection of 2-chlorothiolphenol. A dramatic SERS enhancement was observed on clustered AgMFs because of the synergic coupling of hot-spots that were attributed to the roughened nanoedge assemblies on individual particle and interparticle junctions between AgMFs. The resultant AgMFs endowed with unique morphology demonstrated highly sensitive SERS substrates, warranting highly sensitive detection of probing molecules due to hierarchical surface roughness which can also make it possible to monitor plasmon-driven surface reactions.

■ ASSOCIATED CONTENT

Ⓢ Supporting Information

XPS and EDX spectra of as-prepared AgMFs (Figure S1), UV−vis spectra of AgMFs prepared by different chitosan concentrations and different amounts of $AgNO_3$ (Figure S2), Raman spectra of 2-chlorothiophenol (CTP, 99% solution) (Figure S3), and Raman spectra of 4-aminothiophenol (ATP, 10^{-4} M) adsorbed on different AgMFs and their corresponding SEM images (Figure S4). This material is available free of charge via the Internet at http://pubs.acs.org.

■ AUTHOR INFORMATION

Corresponding Author

*Tel: +82-31-7505360. E-mail: lswha@gachon.ac.kr.

Notes

The authors declare no competing financial interest.

■ ACKNOWLEDGMENTS

This work was supported by the National Research Foundation of Korea (NRF) grant funded by the Korea government (MEST) (No. 20090093908) and by the National Research Foundation of Korea Grant funded by the Korean Government (MEST) (NRF-2010-C1AAA001-2010-0028958).

■ REFERENCES

(1) Campion, A.; Kambhampati, P. Surface-Enhanced Raman Scattering. *Chem. Soc. Rev.* **1998**, *27*, 241−250.

(2) Kambhampati, P.; Child, C.; Foster, M. C.; Campion, A. On the Chemical Mechanism of Surface Enhanced Raman Scattering: Experiment and Theory. *J. Chem. Phys.* **1998**, *108*, 5013−5026.

(3) Kneipp, K.; Kneipp, H.; Itzkan, I.; Dasari, R. R.; Feld, M. S. Surface-Enhanced Raman Scattering and Biophysics. *J. Phys.: Condens. Matter* **2002**, *14*, 597.

(4) Stiles, P. L.; Dieringer, J. A.; Shah, N. C.; Van Duyne, R. P. Surface-Enhanced Raman Spectroscopy. *Annu. Rev. Anal. Chem.* **2008**, *1*, 601−626.

(5) Wang, H.; Halas, N. J. Mesoscopic Au "Meatball" Particles. *Adv. Mater.* **2008**, *20*, 820−825.

(6) Liang, H.; Li, Z.; Wang, W.; Wu, Y.; Xu, H. Highly Surface-Roughened "Flower-like" Silver Nanoparticles for Extremely Sensitive

Substrates of Surface-Enhanced Raman Scattering. *Adv. Mater.* **2009**, *21*, 4614−4618.
(7) Potara, M.; Baia, M.; Farcau, C.; Astilean, S. Chitosan-Coated Anisotropic Silver Nanoparticles as a SERS Substrate for Single-molecule Detection. *Nanotechnology* **2012**, *23*, No. 055501.
(8) Sajanlal, P. R.; Pradeep, T. Mesoflowers: A New Class of Highly Efficient Surface-Enhanced Raman Active and Infrared-Absorbing Materials. *Nano Res.* **2009**, *2*, 306−320.
(9) Bechelany, M.; Brodard, P.; Elias, J.; Brioude, A.; Michler, J.; Philippe, L. Simple Synthetic Route for SERS-Active Gold Nanoparticles Substrate with Controlled Shape and Organization. *Langmuir* **2010**, *26*, 14364−14371.
(10) Xu, D.; Gu, J.; Wang, W.; Yu, X.; Xi, K.; Jia, X. Development of Chitosan-coated Gold Nanoflowers as SERS-Active Probes. *Nanotechnology* **2010**, *21*, No. 375101.
(11) Jena, B. K.; Mishra, B.; Bohidar, S. Synthesis of Branched Ag Nanoflowers based on a Bioinspired Technique: Their Surface enhanced Raman Scattering and Antibacterial Activity. *J. Phys. Chem. C* **2009**, *113*, 14753−14758.
(12) Sau, T. K.; Murphy, C. J. Seeded High Yield Synthesis of Short Au Nanorods in Aqueous Solution. *Langmuir* **2004**, *20*, 6414−6420.
(13) Sperling, R.; Parak, W. Surface Modification, Functionalization and Bioconjugation of Colloidal Inorganic Nanoparticles. *Philos. Trans. R. Soc., A* **2010**, *368*, 1333−1383.
(14) Millstone, J. E.; Park, S.; Shuford, K. L.; Qin, L.; Schatz, G. C.; Mirkin, C. A. Observation of a Quadrupole Plasmon Mode for a Colloidal Solution Of Gold Nanoprisms. *J. Am. Chem. Soc.* **2005**, *127*, 5312−5313.
(15) Han, Y.; Liu, S.; Han, M.; Bao, J.; Dai, Z. Fabrication of Hierarchical Nanostructure of Silver via a Surfactant-Free Mixed Solvents Route. *Cryst. Growth Des.* **2009**, *9*, 3941−3947.
(16) Wang, L.; Li, H.; Tian, J.; Sun, X. Monodisperse, Micrometer-Scale, Highly Crystalline, Nanotextured Ag Dendrites: Rapid, Large-Scale, Wet-Chemical Synthesis and Their Application as SERS Substrates. *ACS Appl. Mater. Interfaces* **2010**, *2*, 2987−2991.
(17) Xie, S.; Zhang, X.; Xiao, D.; Paau, M. C.; Huang, J.; Choi, M. M. Fast Growth Synthesis of Silver Dendrite Crystals Assisted by Sulfate Ion and its Application for Surface-Enhanced Raman Scattering. *J. Phys. Chem. C* **2011**, *115*, 9943−9951.
(18) Huang, D.; Qi, Y.; Bai, X.; Shi, L.; Jia, H.; Zhang, D.; Zheng, L. One-Pot Synthesis of Dendritic Gold Nanostructures in Aqueous Solutions of Quaternary Ammonium Cationic Surfactants: Effects of the Head Group and Hydrocarbon Chain Length. *ACS Appl. Mater. Interfaces* **2012**, *4*, 4665−4671.
(19) Noroozi, M.; Zakaria, A.; Moksin, M. M.; Wahab, Z. A.; Abedini, A. Green Formation of Spherical and Dendritic Silver Nanostructures under Microwave Irradiation without Reducing Agent. *Int. J. Mol. Sci.* **2012**, *13*, 8086−8096.
(20) Wang, X.; Liu, X. Self-Assembled Synthesis of Ag Nanodendrites and Their Applications To SERS. *J. Mol. Struct.* **2011**, *997*, 64−69.
(21) Rashid, M. H.; Mandal, T. K. Synthesis and Catalytic Application of Nanostructured Silver Dendrites. *J. Phys. Chem. C* **2007**, *111*, 16750−16760.
(22) Huang, J.; Vongehr, S.; Tang, S.; Lu, H.; Shen, J.; Meng, X. Ag Dendrite-Based Au/Ag Bimetallic Nanostructures with Strongly Enhanced Catalytic Activity. *Langmuir* **2009**, *25*, 11890−11896.
(23) Mdluli, P.; Revaprasadu, N. Time Dependant Evolution of Silver Nanodendrites. *Mater. Lett.* **2009**, *63*, 447−450.
(24) Lee, G.-J.; Shin, S.-I.; Oh, S.-G. Preparation of Silver Dendritic Nanoparticles Using Sodium Polyacrylate in Aqueous Solution. *Chem. Lett.* **2004**, *33*, 118−119.
(25) Sun, X.; Hagner, M. Novel Preparation of Snowflake-like Dendritic Nanostructures of Ag or Au at Room Temperature via A Wet-Chemical Route. *Langmuir* **2007**, *23*, 9147−9150.
(26) Ren, W.; Guo, S.; Dong, S.; Wang, E. A Simple Route for the Synthesis of Morphology-Controlled and SERS-Active Ag Dendrites with Near-Infrared Absorption. *J. Phys. Chem. C* **2011**, *115*, 10315−10320.
(27) Yang, Z.; Chiu, T.-C.; Chang, H.-T. Preparation and Characterization of Different Shapes Of Silver Nanostructures in Aqueous Solution. *Open Nanosci. J.* **2007**, *1*, 5−12.
(28) Zhu, L.-P.; Zhang, W.-D.; Xiao, H.-M.; Yang, Y.; Fu, S.-Y. Facile Synthesis of Metallic Co-hierarchical Nanostructured Microspheres by a Simple Solvothermal Process. *J. Phys. Chem. C* **2008**, *112*, 10073−10078.
(29) Wang, W.; Yang, X.; Cui, H. Growth Mechanism of Flowerlike Gold Nanostructures: Surface Plasmon Resonance (SPR) and Resonance Rayleigh Scattering (RRS) Approaches to Growth Monitoring. *J. Phys. Chem. C* **2008**, *112*, 16348−16353.
(30) Wang, Y.; Yan, B.; Chen, L. SERS Tags: Novel Optical Nanoprobes for Bioanalysis. *Chem. Rev.* **2012**, *113*, 1391−1428.
(31) Huang, Y.-F.; Zhu, H.-P.; Liu, G.-K.; Wu, D.-Y.; Ren, B.; Tian, Z.-Q. When the Signal is not from the Original Molecule to be Detected: Chemical Transformation of Para-Aminothiophenol on Ag during The SERS Measurement. *J. Am. Chem. Soc.* **2010**, *132*, 9244−9246.
(32) Xu, P.; Kang, L.; Mack, N. H.; Schanze, K. S.; Han, X.; Wang, H.-L., Mechanistic Understanding of Surface Plasmon assisted Catalysis on a Single Particle: Cyclic Redox Of 4-Aminothiophenol. *Sci. Rep.* **2013**, *3*.
(33) Boca, S.; Rugina, D.; Pintea, A.; Barbu-Tudoran, L.; Astilean, S. Flower-Shaped Gold Nanoparticles: Synthesis, Characterization and their Application as SERS-Active Tags inside Living Cells. *Nanotechnology* **2011**, *22*, No. 055702.
(34) Liu, T.; Li, D.; Yang, D.; Jiang, M. Fabrication of Flower-like Silver Structures through Anisotropic Growth. *Langmuir* **2011**, *27*, 6211−6217.
(35) Song, H. M.; Deng, L.; Khashab, N. M. Intracellular Surface-Enhanced Raman Scattering (SERS) with Thermally Stable Gold Nanoflowers Grown From Pt And Pd Seeds. *Nanoscale* **2013**, *5*, 4321−4329.
(36) Zhang, M.; Zhao, A.; Sun, H.; Guo, H.; Wang, D.; Li, D.; Gan, Z.; Tao, W. Rapid, Large-Scale, Sonochemical Synthesis of 3D Nanotextured Silver Microflowers as Highly Efficient SERS Substrates. *J. Mater. Chem.* **2011**, *21*, 18817−18824.
(37) Personick, M. L.; Mirkin, C. A. Making Sense of the Mayhem behind Shape Control in the Synthesis of Gold Nanoparticles. *J. Am. Chem. Soc.* **2013**, *135*, 18238−18247.
(38) Xia, Y.; Xiong, Y.; Lim, B.; Skrabalak, S. E. Shape-Controlled Synthesis of Metal Nanocrystals: Simple Chemistry Meets Complex Physics? Angew. *Chem. Int. Ed.* **2009**, *48*, 60−103.
(39) Nhung, T. T.; Bu, Y.; Lee, S.-W. Facile Synthesis of Chitosan-Mediated Gold Nanoflowers as Surface-Enhanced Raman Scattering (SERS) Substrates. *J. Cryst. Growth* **2013**, *373*, 132−137.
(40) Jung, K.; Hahn, J.; In, S.; Bae, Y.; Lee, H.; Pikhitsa, P. V.; Ahn, K.; Ha, K.; Lee, J. K.; Park, N. Hotspot-Engineered 3D Multipetal Flower Assemblies for Surface-Enhanced Raman Spectroscopy. *Adv. Mater.* **2014**.
(41) Iravani, S. Green Synthesis of Metal Nanoparticles Using Plants. *Green Chem.* **2011**, *13*, 2638−2650.
(42) Fang, J.; You, H.; Zhu, C.; Kong, P.; Shi, M.; Song, X.; Ding, B. Thermodynamic and Kinetic Competition in Silver Dendrite Growth. *Chem. Phys. Lett.* **2007**, *439*, 204−208.
(43) Chen, A.; Peng, X.; Koczkur, K.; Miller, B. Super-Hydrophobic Tin Oxide Nanoflowers. *Chem. Commun.* **2004**, 1964−1965.
(44) Dong, Y.; Ruan, Y.; Wang, H.; Zhao, Y.; Bi, D. Studies on Glass Transition Temperature of Chitosan with Four Techniques. *J. Appl. Polym. Sci.* **2004**, *93*, 1553−1558.
(45) Kharisov, B. I. A Review for Synthesis of Nanoflowers. *Recent Pat. Nanotechnol.* **2008**, *2*, 190−200.
(46) Jiang, X.; Chen, W.; Chen, C.; Xiong, S.; Yu, A. Role of Temperature in the Growth of Silver Nanoparticles Through a Synergetic Reduction Approach. *Nanoscale Res. Lett.* **2011**, *6*, 32.
(47) Yang, J.; Dennis, R. C.; Sardar, D. K. Room-Temperature Synthesis of Flowerlike Ag Nanostructures Consisting of Single Crystalline Ag Nanoplates. *Mater. Res. Bull.* **2011**, *46*, 1080−1084.

(48) ShuangáShen, X.; ZhongáWang, G. Nanospheres of Silver Nanoparticles: Agglomeration, Surface Morphology Control and Application as SERS Substrates. *Phys. Chem. Chem. Phys.* **2009**, *11*, 7450−7454.
(49) Chen, S.; Carroll, D. L. Synthesis and Characterization of Truncated Triangular Silver Nanoplates. *Nano Lett.* **2002**, *2*, 1003−1007.
(50) Orendorff, C. J.; Gole, A.; Sau, T. K.; Murphy, C. J. Surface-Enhanced Raman Spectroscopy of Self-Assembled Monolayers: Sandwich Architecture and Nanoparticle Shape Dependence. *Anal. Chem.* **2005**, *77*, 3261−3266.
(51) Mayer, K. M.; Hafner, J. H. Localized Surface Plasmon Resonance Sensors. *Chem. Rev.* **2011**, *111*, 3828−3857.
(52) Zhang, J. Z. *Optical Properties and Spectroscopy of Nanomaterials*; World Scientific: Hackensack, NJ, 2009.
(53) Zhang, W.; Qiao, X.; Chen, J.; Wang, H. Preparation of Silver Nanoparticles in Water-In-Oil AOT Reverse Micelles. *J. Colloid Interface Sci.* **2006**, *302*, 370−373.
(54) Wang, Y.; Chen, H.; Wang, E. Facile Fabrication of Gold Nanoparticle Arrays for Efficient Surface-Enhanced Raman Scattering. *Nanotechnology* **2008**, *19*, 105604.
(55) Jia, W.; Li, J.; Jiang, L. Synthesis of Highly Branched Gold Nanodendrites with a Narrow Size Distribution and Tunable NIR and SERS Using a Multiamine Surfactant. *ACS Appl. Mater. Interfaces* **2013**, *5*, 6886−6892.
(56) Bu, Y.; Lee, S. Influence of Dopamine Concentration and Surface Coverage of Au Shell on the Optical Properties of Au, Ag, and $Ag_{core}Au_{shell}$ Nanoparticles. *ACS Appl. Mater. Interfaces* **2012**, *4*, 3923−3931.
(57) Bechelany, M.; Brodard, P.; Philippe, L.; Michler, J. Extended Domains of Organized Nanorings of Silver Grains as Surface-Enhanced Raman Scattering Sensors for Molecular Detection. *Nanotechnology* **2009**, *20*, No. 455302.
(58) Linn, N. C.; Sun, C.-H.; Arya, A.; Jiang, P.; Jiang, B. Surface-Enhanced Raman Scattering on Periodic Metal Nanotips with Tunable Sharpness. *Nanotechnology* **2009**, *20*, No. 225303.
(59) Jiang, P.; Deng, K.; Fichou, D.; Xie, S.-S.; Nion, A.; Wang, C. STM Imaging Ortho-and Para-Fluorothiophenol Self-Assembled Monolayers on Au (111). *Langmuir* **2009**, *25*, 5012−5017.
(60) Nishi, N.; Hobara, D.; Yamamoto, M.; Kakiuchi, T. Orientation of O-, M-, and P-Methylbenzylmercaptans Adsorbed on Au (111) Probed by Broad-Bandwidth Sum Frequency Generation Spectroscopy. *Langmuir* **2003**, *19*, 6187−6192.
(61) Wang, Y.; Chen, H.; Dong, S.; Wang, E. Surface Enhanced Raman Scattering of P-Aminothiophenol Self-Assembled Monolayers in Sandwich Structure Fabricated on Glass. *J. Chem. Phys.* **2006**, *124*, 74709−74709.
(62) Nehl, C. L.; Liao, H.; Hafner, J. H. Optical Properties of Star-Shaped Gold Nanoparticles. *Nano Lett.* **2006**, *6*, 683−688.
(63) Ye, J.; Hutchison, J. A.; Uji-i, H.; Hofkens, J.; Lagae, L.; Maes, G.; Borghs, G.; Van Dorpe, P. Excitation Wavelength Dependent Surface Enhanced Raman Scattering of 4-Aminothiophenol on Gold Nanorings. *Nanoscale* **2012**, *4*, 1606−1611.
(64) Christou, K.; Knorr, I.; Ihlemann, J. r.; Wackerbarth, H.; Beushausen, V. Fabrication and Characterization of Homogeneous Surface-Enhanced Raman Scattering Substrates by Single Pulse UV-Laser Treatment Of Gold And Silver Films. *Langmuir* **2010**, *26*, 18564−18569.
(65) Kang, L.; Xu, P.; Chen, D.; Zhang, B.; Du, Y.; Han, X.; Li, Q.; Wang, H.-L. Amino Acid-Assisted Synthesis of Hierarchical Silver Microspheres for Single Particle Surface-Enhanced Raman Spectroscopy. *J. Phys. Chem. C* **2013**, *117*, 10007−10012.